Electronic Supplementary Material (ESI) for Journal of Materials Chemistry C.

Supporting information

Au nanorods characterization and setup schematic

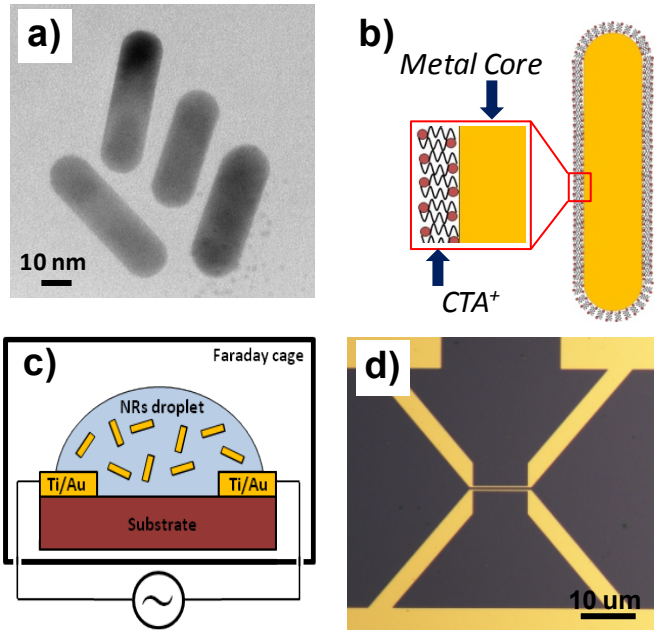

Figure S1 : a) TEM image of the as-prepared Au-NRs. b) Schematic picture of the multilayer structure of the chemical-syntetized Au-NRs c) Schematic representation of the set-up used in dielectrophoretic process d) Optical image of Ti/Au electrodes separated by 2 um gap on Si/SiO_2 substrate

Calculation of the Clausius-Mossotti factor for core-shell Au nanorods

The Clausius-Mossotti factor $\tilde{f}_a(\omega)$ along the main axis a was calculated by the following expression

$$\tilde{f}_a(\omega) = \frac{\tilde{\varepsilon}_p(\omega) - \tilde{\varepsilon}_m(\omega)}{3((\tilde{\varepsilon}_p(\omega) - \tilde{\varepsilon}_m(\omega))L_a + \tilde{\varepsilon}_m(\omega))} \quad \text{(s1)}$$

Where the complex permittivity of water is $\tilde{\varepsilon}_m(\omega) = \varepsilon_m + \sigma_m / j\omega$ with ε_m and $\sigma_m = 4 \cdot 10^{-5}$ S/m respectively the permittivity and conductivity of the medium, j the imaginary number, ω the frequency of the electric field. The particle was approximated to a shelled ellipsoid with an outer equatorial radius a_1, inner equatorial radius a_2 = 7nm, an outer polar radius b_1 and an inner polar radius b_2 =21nm. We assumed that the inner and outer spheroid share the same foci. The complex permittivity of core-shell ellipsoidal particles $\tilde{\varepsilon}_{p,\alpha}(\omega)$ was calculated from the values of the complex permittivity of the core $\tilde{\varepsilon}_c(\omega)$ and the shell $\tilde{\varepsilon}_s(\omega)$ by using[1]

$$\tilde{\varepsilon}_{p,\alpha}(\omega) = \tilde{\varepsilon}_s(\omega) \frac{\tilde{\varepsilon}_s(\omega) + (\tilde{\varepsilon}_c(\omega) - \tilde{\varepsilon}_s(\omega))[L_{1,\alpha} + \nu_1(1 - L_{2,\alpha})]}{\tilde{\varepsilon}_s(\omega) + (\tilde{\varepsilon}_c(\omega) - \tilde{\varepsilon}_s(\omega))(L_{1,\alpha} - \nu_1 L_{2,\alpha})} \quad \text{(s2)}$$

where $L_{1,a}$ =0.109 and $L_{2,a}$ are the depolarizing factor referred to the core ellipsoid with axis a_1, b_1 and shell ellipsoid with axis a_2, b_2 and $\nu_1 = a_1 b_1^2 / a_2 b_2^2$.

Regarding the permittivity of the shell, we notice that although the permittivity for organic molecules is around $5\varepsilon_0$, dielectric constant of cell membranes[1] can be as large as $10\varepsilon_0$ or more. CTAB molecules form a positively charged double layer around the metal surface that induces counter-ions adsorption on the layer surface. Due to the complexity of this structure the conductivity and dielectric constant could sensibly deviate from the value for the organic molecule towards a response more typical of cell membrane.

The discussion about the effective values of permittivity and conductivity for the metal core requires more careful considerations. The general relation between complex permittivity and conductivity is[2]

$$\tilde{\varepsilon}(\omega) = 1 + i\tilde{\sigma}(\omega)/\omega$$

where

$$\tilde{\varepsilon}(\omega) = \varepsilon^{'}(\omega) + i\varepsilon^{''}(\omega)$$

$$\tilde{\sigma}(\omega) = \sigma^{'}(\omega) + i\sigma^{''}(\omega)$$

with $\tilde{\varepsilon}(\omega)$ the complex permittivity, $\tilde{\sigma}(\omega)$ the complex conductivity and *i* the imaginary number and ω the electric field frequency.

For ultra-low frequencies the conductivity of the metal is almost real, as expected for a perfect conductor, so within this approximation we can assume the complex permittivity of gold as

$$\varepsilon(\omega) \approx 1 + i\sigma_0/\omega$$

with σ_0 independent from the frequency. If we use the DC conductivity of bulk gold (~4 10^8 S/m) the first sharp decreasing of particle density at 100kHz-1MHz can be well reproduced. However, the second dispersion at 50 MHz cannot be fitted. The frequency at which this dispersion occurs is mainly determined by the conductivity of the metal core. Using the conductivity of bulk gold the dispersion appears at frequency of 10^{11}-10^{12} Hz outside the explored range. The change of sign of the real part of Clausius-Mossotti factor in correspondence of the second dispersion is critical to explain why no particle deposition was observed above 50 MHz independently of the intensity of the electric field applied. For this reason we fitted the data using σ_0 as free parameter and we obtained the value of 0.43±0.05 S/m that well reproduced the experimental data. Moreover in order to take into account the effect of surfactant molecules, ions and colloidal particles on the dielectric

constant of the surrounding medium (ε_{medium}) we included this parameter in the fit. We used $\varepsilon_{core} = 1\varepsilon_0$ and $\sigma_{medium} = 4 \cdot 10^{-5}$ S/m.

The Clausius-Mossotti function was obtained by fitting the surface density of particle measured at different frequency with the following expression

$$\rho_s(\varepsilon_s, \varepsilon_c, \sigma_s, \sigma_c, b_1, \omega) = A \cdot \mathrm{Re}[\tilde{f}_a(\varepsilon_s, \varepsilon_c, \sigma_s, \sigma_c, b_1, \omega)] \quad \text{(s3)}$$

where $\varepsilon_s, \varepsilon_c, \sigma_s, \sigma_c, b_1$ and A are the free parameters of the model. Experimental data of figure 2b was fitted by applying the least-square fitting procedure. Data trend was well reproduced and from the best fit we obtained the following estimation for the free parameters:

$\varepsilon_{shell} = 12.8 \pm 0.7\ \varepsilon_0$

$\sigma_{shell} = 8.7 \pm 0.5\ 10^{-5}$ S/m

$\varepsilon_{medium} = 93 \pm 2\ \varepsilon_0$

$\sigma_{core} = 0.43 \pm 0.05$ S/m

$b_2 = 11.3 \pm 0.6$ nm

$A = 3.58 \cdot 10^3$

The core-shell model proposed by the authors is a simplified picture of a very complex system that in general required an electrokinetic model for a more satisfactory description. Nevertheless the simply core-shell model presented was able to describe the main features. However, the principal limitations of the core-shall structure are the oversimplification of the surrounding medium properties (due to the presence of molecules, ions and colloidal particles) and the internal structure of the shell (that include a double CTAB layer and counterions layer adsorbed on the surface). From the mathematical formulation of our model, the build-up of charge at each interface determines a dielectric dispersion. Therefore in a core-shell structure only two dielectric dispersions can be

obtained. The sharp variation of density at 30 MHz would require a second shell to be mathematically described. However, the intensity of that peak was found weak and largely variable in different colloidal batches thus it was considered negligible in first approximation. Moreover such variability as well as the observed electrical shorts obtained at that frequency suggests attributing the peak to the properties of the surrounding medium more than the particle itself.

Electric field simulation and assembly mechanism

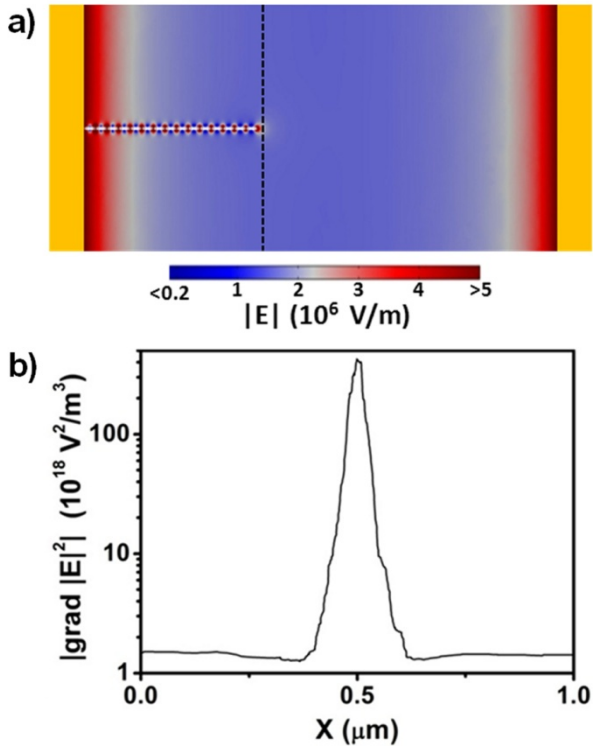

Figure S2. (a) Finite element method simulation of electric field magnitude inside a 2 μm gap on Si/SiO_2 substrate and around a chain of aligned metal rods for an applied voltage of 4.2 $V_{rms;}$ (b) Plot of the E-field magnitude gradient along the dotted line shown in (a).

Finite element method simulations of electric field distribution across 2 μm electrode gap have been undertaken (Figure S2) to illustrate the formation of localized high E-field areas leading to ordered alignment of nanorods. Simulations were undertaken using commercial finite element software

package Comsol Multiphysics 4.1. (COMSOL, SE). The 3D geometry consisted of two electrodes 200 nm width, 1 μm long and 50 nm thick separated by 2 μm on top of Si/SiO_2 (300 nm) substrate $\varepsilon_m = 3.9\varepsilon_0$. The nanorod was modeled as a perfect conductor with a cylindrical body (radius 7 nm and length 28 nm) and two hemispherical caps (radius 7 nm). The electrodes and particles were covered by 100 μm thick water layer ($\varepsilon_m = 80\varepsilon_0$) with an applied voltage of 4.2 V_{rms} (E= 1.48×10^6 V/m in the center of the gap) across the electrodes. Floating condition were applied to the Si boundary and the Neumann condition on the other external boundary. As showed in figure S1a, for an applied voltage, the associated electric field was highest in proximity of the electrode edges. Therefore, an isolated nanorod in solution could move towards the electrode edges, until a physical contact was established with the metal electrode. As consequence, generation of a localized high E-field gradient occurred at the nanorod outer edge (see profile in Figure S1b) that promoted the assembly of subsequent nanorods into 1D chains. It should be noted that this condition corresponded to the application of a macroscopic F_{DEP} below the threshold required for nanorod deposition. However formation of localized E-field areas where F_{DEP} was greater than the threshold force, promoted selective assembly of nanorods into head-to-tail architectures.

The macroscopic applied electric field induces a dipole on the nanorod proportional to the field intensity. Consequently the local electric field in proximity of the nanorod has dipole symmetry with intensity given by the linear superposition of the dipole field and the spatially homogeneous macroscopic field. Therefore two parallel nanorods have the induced dipole oriented in the same direction giving rise to a repulsion force preventing the side-by-side assembly. Moreover the head-totail assembly was explained on the basis of dielectrophoresis driven by the enhanced field at the nanorod, as demonstrated by FEM simulations. However we should notice that in the presented assembly mechanism discussed in the paper we assumed that torque force acting on the nanorod-

dipole aligns the main axis of the particle to the external electric field. To proof this hypothesis we calculated the torque force from the Clausius-Mossotti factor using the expression

$$\langle \mathrm{T} \rangle_z = \frac{2}{3}\pi a b^2 \varepsilon_m (L_\perp - L_\parallel)\,\mathrm{Re}[\tilde{f}_\perp \cdot \tilde{f}_\parallel]\, E_\parallel E_\perp$$

Where the suffix $\perp$ and $\parallel$ indicate the component of the depolarizing factor, Clausius-Mossotti factor and electric field perpendicular and parallel respect to the main axis of the nanorod. In the explored range of frequencies (100 kHz-50MHz) the torque force was found having a negative value that indicates a stable configuration with the main axes aligned respect to the electric field (see figure S2). The torque force is expected to change sign below 100-200 kHz. However at this low frequency range electrical shortcuts during the assembly process prevented a satisfactory investigation (figure S2b).

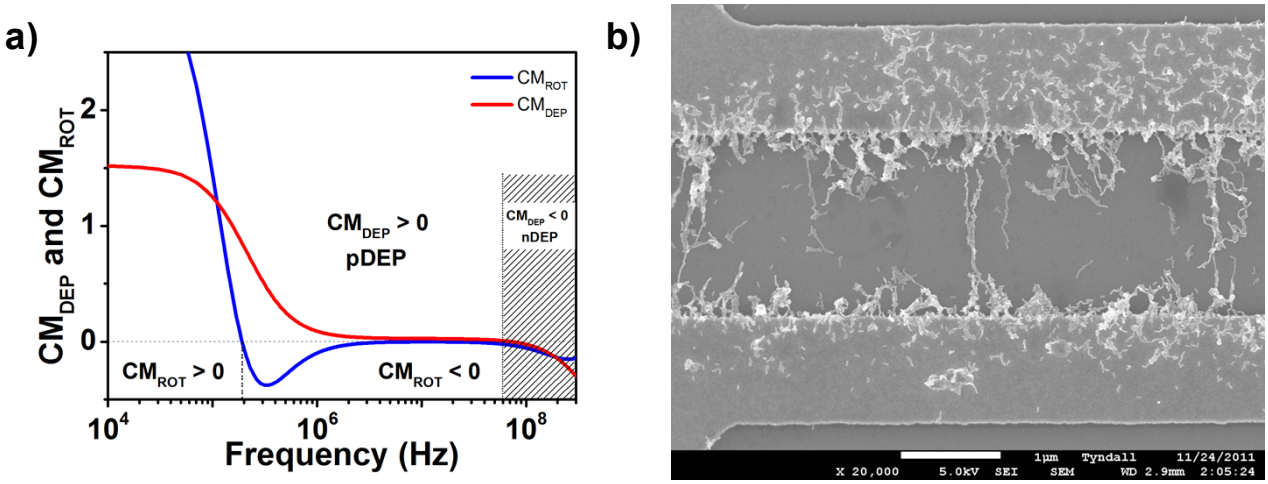

Figure S3. a) Calculated real part of the Clausius-Mossotti factor (CM) and coefficient $\mathrm{Re}[\tilde{f}_\perp \cdot \tilde{f}_\parallel]$ (CM_{ROT}) showing the behavior of dielectrophoretic force and torque force respectively. Negative values of the CM indicates negative dielectrophoresis instead positive values indicates positive dielectrophoresis. Analogously negative values of the torque force implicate a stable configuration with the main axes of the nanorod aligned along the electric field lines whereas positive values a preferred alignment of the short axes. b) SEM image of a nanorod deposition obtaind at 100kHz

with 10Vpp applied. At this frequency the model predicts a side-by-side alignment of nanorods but a clear evidence of this assembly was not observed.

Nanorods alignment

Comparing the dipole energy with the thermal energy of the particles the minimum electric field strength necessary to obtain an observable nanorod alignment is given by:

$$p \cdot E \approx \frac{3}{2} kT \qquad (1)$$

where k is the Boltzman constant and p is the effective dipole moment along the nanorod long axis defined by:

$$p = 3V\varepsilon_m Re[\tilde{f}_\alpha(\omega)]E \qquad (2)$$

Using T = 290 K we obtain $E_{min} = 2 \cdot 10^5$ V/m, that is one order of magnitude lower than the electric field ($\sim 2 \cdot 10^6$ V/m) applied experimentally. Figure S2 shows SEM images of deposited Au Nanorods with correlated angular distribution histograms.

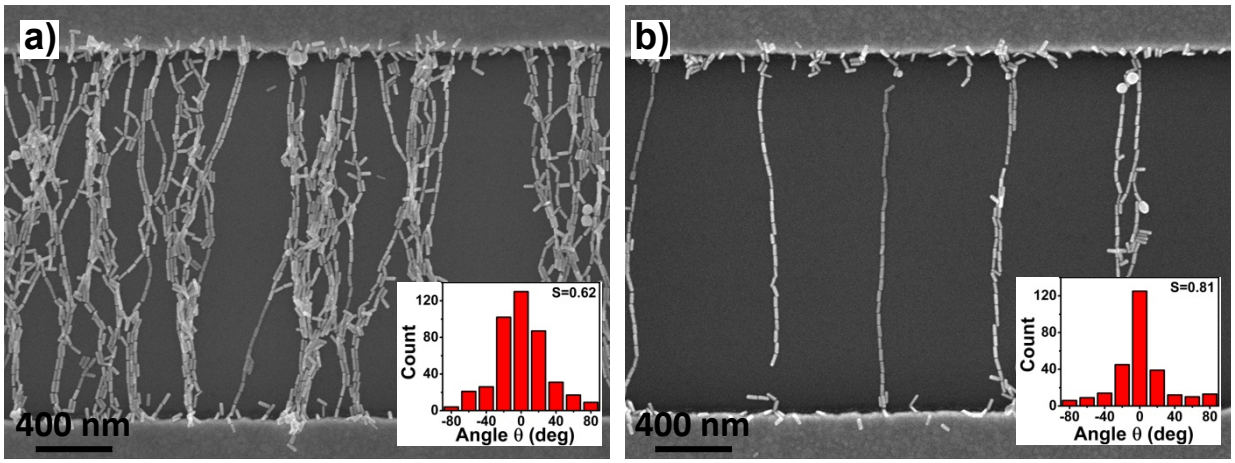

Figure S4. SEM images showing electric field deposition of Au nanorods at the following deposition conditions: a) E=2.20×10^6 V/m, 15 MHz; b) E=1.72×10^6 V/m, 15 MHz; Insets: angular distribution of Au nanorods along the applied E-field direction.

1. Hu, Q.; Joshi, R. P.; Beskok, A., Model study of electroporation effects on the dielectrophoretic response of spheroidal cells. *J. Appl. Phys.* **2009,** *106* (2), 024701-8.
2. Maier, S. A., *Plasmonics: Fundamentals and Applications: Fundamentals and Applications*. Springer: 2007.